Author(s): Radevici, Ivan & Tiira, Jonna & Oksanen, Jani

Title: Lock-in thermography approach for imaging the efficiency of light emitters and optical coolers

Year: 2017

Version: Post print

Please cite the original version:

Radevici, Ivan & Tiira, Jonna & Oksanen, Jani. 2017. Lock-in thermography approach for imaging the efficiency of light emitters and optical coolers. SPIE Proceedings. Volume 10121. 7. DOI: 10.1117/12.2249978.

Lock-in thermography approach for imaging the efficiency of light emitters and optical coolers

Ivan Radevici[a], Jonna Tiira[a], and Jani Oksanen[a]

[a]Aalto University, P.O. Box 12200, FI-00076, Finland

ABSTRACT

Developing optical cooling technologies requires access to reliable efficiency measurement techniques and ability to detect spatial variations in the efficiency and light emission of the devices. We investigate the possibility to combine the calorimetric efficiency measurement principles with lock-in thermography (LIT) and conventional luminescence microscopy to enable spatially resolved measurement of the efficiency, current spreading and local device heating of double diode structures (DDS) serving as test vessels for developing thermophotonic cooling devices. Our approach enables spatially resolved characterization and localization of the losses of the double diode structures as well as other light emitting semiconductor devices. In particular, the approach may allow directly observing effects like current crowding and surface recombination on the light emission and heating of the DDS devices.

—Published in the proceedings of SPIE, Photonics West 2017–

Keywords: electroluminescent cooling, quantum efficiency, lock-in thermography, radiative and non-radiative recombination, III-V semiconductors, double diode structures, efficiency nonuniformity, surface states

1. INTRODUCTION

For both the physics and the engineering of devices such as semiconductor lasers, LEDs and other emerging devices based on high efficiency light emission such as laser coolers or optical heat pumps,[1,2] it is crucial to be able to accurately quantify the device efficiency and the loss mechanisms leading to non-radiative recombination. However, sufficiently accurate measurement of the emission efficiency of light emitting materials and devices, conventionally carried out using carefully calibrated integrating spheres and radiometric techniques, becomes increasingly complicated in high efficiency applications where even small calibration errors may lead to incorrect conclusions about device performance - especially when trying to detect near unity efficiencies in developing optical cooling technologies.

To solve the conventional calibration challenges, the optical cooling community has developed calorimetric efficiency measurement techniques where relative measurements of light emission and device heating are used to enable fully calibrated efficiency measurements.[3] This approach relies on energy conservation stating that any power provided to the sample must be converted into either light or heat. The calorimetric efficiency measurement has been applied using various temperature measurement techniques such as photoacoustic techniques, thermistors or changes in the peak position of photoluminescence.[4] As such these techniques have proven very useful, but they only provide spatially averaged information and therefore do not provide information e.g. on the spatial dependence of the light emission efficiency, current crowding, shunts or possible defect induced recombination channels.

In this paper we report our progress in developing thermal imaging and calorimetric approaches to analyze the current spreading and efficiency of the double diode structures (DDS) we have recently introduced as a test devices for thermophotonic cooling.[5] To this end we combine the calorimetric efficiency measurement techniques with lock-in thermography (LIT) method[6] that is normally used for very sensitive detection of spatial temperature variations, defects and shunts in electronic devices. In contrast to previous techniques, combining the thermal images obtained using the lock-in thermography technique with spatially resolved photoluminescence images is

Corresponding author: I. Radevici
E-mail: ivan.radevici@aalto.fi

expected to allow spatially resolved non-contact characterization of the devices, enabling the measurement of efficiencies in different spots of the device while simultaneously also giving access to information about current spreading as well as to conventional uses of LIT in detecting potential shunts and other hot spots.

2. BASIC PRINCIPLES OF SPATIALLY RESOLVED QE DETECTION

In the original calorimetric efficiency measurements proposed by Dunstan[3] the radiative η_r and thermal η_{nr} efficiencies of the device were written as functions of the input power P, photocurrent L_{ext} through an external photodetector and the sample heating power (here change in sample temperature ΔT) as

$$\begin{aligned} \frac{L_{ext}(P)}{P} &= \alpha\eta_r(P) \\ \frac{\Delta T(P)}{P} &= \beta\eta_{nr}(P) \end{aligned} \tag{1}$$

where α and β are unknown calibration constants that depend on the sample as well as on the characteristics of the optical and thermal measurement setup. In Dunstan's approach the calibration constants α and β were then determined by noting that the curves described by Equations (1) must be able to produce a sum of unity when they are properly rescaled.[3] Once the calibration constants were determined the external quantum efficiency (EQE) η_Q could be written as

$$\eta_Q(P) = \frac{eV}{h\nu}\eta_r(P) = \frac{1}{\alpha}\frac{eV}{h\nu}\frac{L_{ext}(P)}{P}. \tag{2}$$

Later this approach has been used and adapted to a number of different purposes and measurement setups involving e.g. thermistors,[7] photoacustic techniques[8] and differential luminescence thermometry,[9] but all of the previous adaptations focus on providing a single averaged efficiency figure for the whole device and neglect both the analysis of the exact conditions for the existence of the solution as well as the possibility of position dependent analysis.

To extend the calorimetric efficiency measurements to spatially resolved measurements of EQE providing a more insightful view of the local device performance and current spreading, we will next reformulate the calorimetric description to a spatially dependent form. In the process we also analyze the conditions for the existence of the solution in more detail using a presentation that also more clearly reflects the energy conserving foundations of the technique than the earlier formulations.

In the position dependent description of the problem we denote the luminescence recorded by a CCD-camera by $L(x,y)$, the thermal signal recorded by an IR-camera in Lock-in mode by $T(x,y)$ and the deposited total power density by $p(x,y)$. While the first two quantities may be experimentally measured with the CCD and thermal cameras, the value $p(x,y)$ for an electrically injected device is only known to fullfill the condition $\int p(x,y)dA = IV$, where the integration is performed over the device area A and I and V denote the total current and applied bias over the device.

The energy conservation requirements used in earlier works also apply locally and therefore the fundamental equations governing the spatially resolved calorimetric measurements are given as

$$p\left(x,y\right) = \phi\left(x,y\right) + q\left(x,y\right) \tag{3a}$$

$$p\left(x,y\right) = a\left(x,y\right)L\left(x,y\right) + b\left(x,y\right)T\left(x,y\right) \tag{3b}$$

$$IV = \int p\left(x,y\right)dA = \int a\left(x,y\right)L\left(x,y\right) + b\left(x,y\right)T\left(x,y\right)dA \tag{3c}$$

where each equation simply states that all injected power either heats up the sample or escapes as light, $a\left(x,y\right)$ is the position dependent calibration constant between the response of the CCD-camera and the radiant flux $\phi\left(x,y\right) = a\left(x,y\right)L\left(x,y\right)$ emitted from location x,y and $b\left(x,y\right)$ is the corresponding calibration coefficient between the thermal signal and the heat flux $q\left(x,y\right) = b\left(x,y\right)T\left(x,y\right)$ heating the sample.

To first analyze when Eq. (3b) has a well defined solution, we formally solve the pair of equations formed by Eq. (3b) and its derivative with respect to some variable S corresponding e.g. to the total input current or power. Omitting the (x, y)-dependence for simplicity, we obtain the solution of the calibration coefficients - which do not depend on S - as

$$\begin{aligned} a &= \left[p(S) \frac{d}{dS} T(S) - T(S) \frac{d}{dS} p(S) \right] W^{-1} \\ b &= \left[L(S) \frac{d}{dS} p(S) - p(S) \frac{d}{dS} L(S) \right] W^{-1} \\ W &= L(S) \frac{d}{dS} T(S) - T(S) \frac{d}{dS} L(S) \end{aligned} \tag{4}$$

where W is the Wronskian of the system of equations formed by Eq. (3b) and its derivative. The calibration coefficients a and b *do not have* a solution only when $W = 0$. Solving the equation $W = 0$ gives the condition $L(S) = CT(S)$ where C is an arbitrary constant. Substituting this condition back to Eq. (3b) results in $p(S) = (a + Cb) L(S)$, directly stating that a solution (4) cannot be found when L and T are directly proportional to p throughout the measurement range. Conversely it also means that whenever conditions where L and T depend nonlinearly on p, the calibration conditions can be inferred from measurements where the system variable S is modified.

While Eq. (3b) can be formally solved e.g. by Eq. (4) or standard linear regression methods, solving the integrated form of the energy conservation Eq. (3c) calls for a slightly more elaborate process. One straightforward option is provided by using standard finite element methods where the device domain is separated into space elements A_i and the calibration coefficients are approximated by using known basis functions $f_i(x, y)$ so that

$$\begin{aligned} a(x, y) &= \Sigma_i a_i f_i(x, y) \\ b(x, y) &= \Sigma_i b_i f_i(x, y) \end{aligned} \tag{5}$$

and the integrated form of the energy conservation law can correspondingly be approximated by the discrete equation

$$IV = \Sigma_{i=1}^{N} a_i \int f_i(x, y) L(x, y) \, dA + b_i \int f_i(x, y) \Delta T(x, y) \, dA. \tag{6}$$

This equation can also be solved using standard regression methods when several measurements m are carried out with different values S_m of a suitable system variable S. Combining the terms of Eq. (6) for different measurements $m = \{1, M\}$ into measurement vector $Y = [IV_1, IV_2, .., IV_M]^T$, calibration coefficient vector $B = [a_1, a_2, ..a_N, b_1, b_2, .., b_N]^T$ and the domain integral values as a matrix consisting of row vectors $X_m = \left[\int f_i(x, y) L_m(x, y) \, dA, \ \int f_i(x, y) T_m(x, y) \, dA \right]$ then allows writing the calibration coefficient vector as

$$B = \left(X^T X \right)^{-1} X^T Y \tag{7}$$

and the quantum efficiency of element i can then be approximated as

$$\eta_i = \frac{e}{\hbar \omega} \frac{a_i \int f_i L dA}{a_i \int f_i L dA + b_i \int f_i T dA}. \tag{8}$$

3. SAMPLE PREPARATION AND EXPERIMENTAL TECHNIQUES

The test devices studied in this work consist of double diode structures (DSS) which include a GaAs and lattice matched GaInP LED grown on top of a photodiode as illustrated in Fig. 1. Fabrication of the epitaxial structures was carried out using molecular beam epitaxy and the epistructures were subsequently processed to contain circular DDS mesas with contact regions providing electrical contacts to the LED and the photodiode.

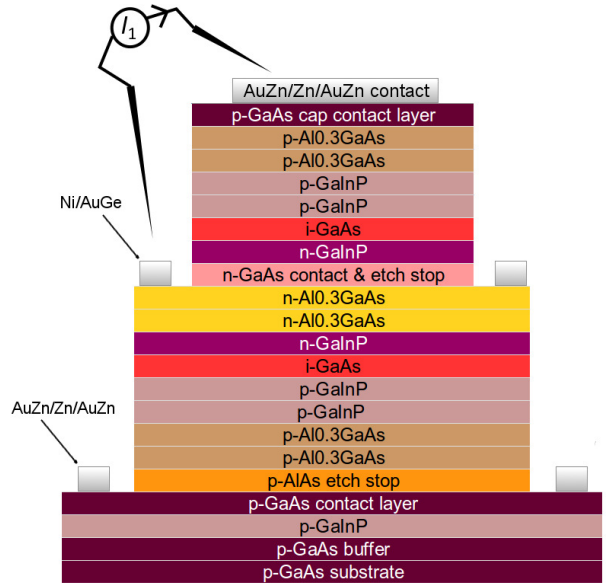

Figure 1. Schematic illustration of the DDS device studied using the thermal and optical cameras. (color online)

Contacts formed on top of the mesa were additionally patterned to contain circular openings to enable imaging of the thermal and optical signals through the semiconductor surface.

The measurements were carried out with a specially designed enhanced LIT setup including a thermal (3-5 μm) and a CMOS (350-1000 nm) cameras and a computer controlled electrical excitation source for pulsed and/or periodic excitation of the samples. For thermal imaging of the DDS structures a lock-in approach was used. Integration time of lock-in measurement was varied from several minutes to 2 hours depending on the excitation power.

4. RESULTS

Figure 2 shows a sequence of the thermal and visible images obtained for injection currents ranging between 10 mA and 100 mA over the 1 mm diameter light emitting DDS mesa. The optical images are simple snapshots taken during the excitation while the thermal images show the magnitude of the Fourier transformed image at the excitation frequency. While the temperature of the contact metal and the semiconductor surfaces are approximately equal within each thermal image, the metal covered parts in the thermal images are clearly visible due to the high reflectivity and low emissivity of the metals. In the optical images, light is only emitted through the parts of the mesa that are not covered by a metal. As can be expected both the heating and light emission increase as the injection current is increased, but there are clear spatial variations in the optical signal strength, most likely due to current crowding in the structure. In addition, for this specific sample, a weak hot-spot is also observed at the upper right edge of the mesa in the thermal images at low current densities and also the probe needles used to contact the mesas partly blur the upper left corners of the mesas and the contact pad on the right.

To further analyze the distribution of heat deposition and the light emission in the structure, we have split the mesa into domains corresponding to the openings made to the metal contacts. Figure 3 shows the light emission and thermal signal as a function of current for four domains corresponding to the central opening (opening #1), the mesa edge (opening #4) and two openings along the line from the center of the mesa to the edge (openings #2 and opening #3, respectively). At large currents the light emission from the central opening is significantly smaller than from the mesa edge, indicating that current crowding becomes an important factor at large currents. The thermal signal, on the other hand, shows that the differences observed in temperature in different openings are quite subtle, and need to be analyzed more carefully.

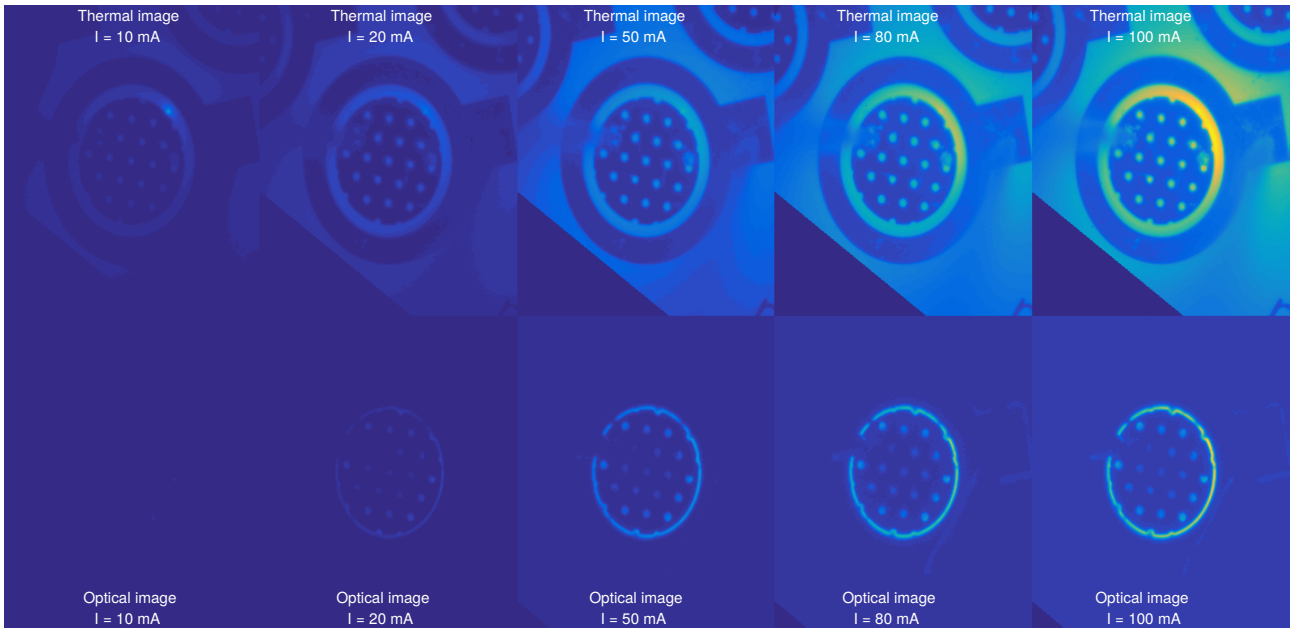

Figure 2. Thermal (top) and visible (bottom) images of the DDS structure for injection currents ranging from 10mA (left) to 100mA (right). The diameter of the light emitting mesa in the figure is 1mm and circular openings where the top metal contacts have been removed have been fabricated on top of the sample. (color online)

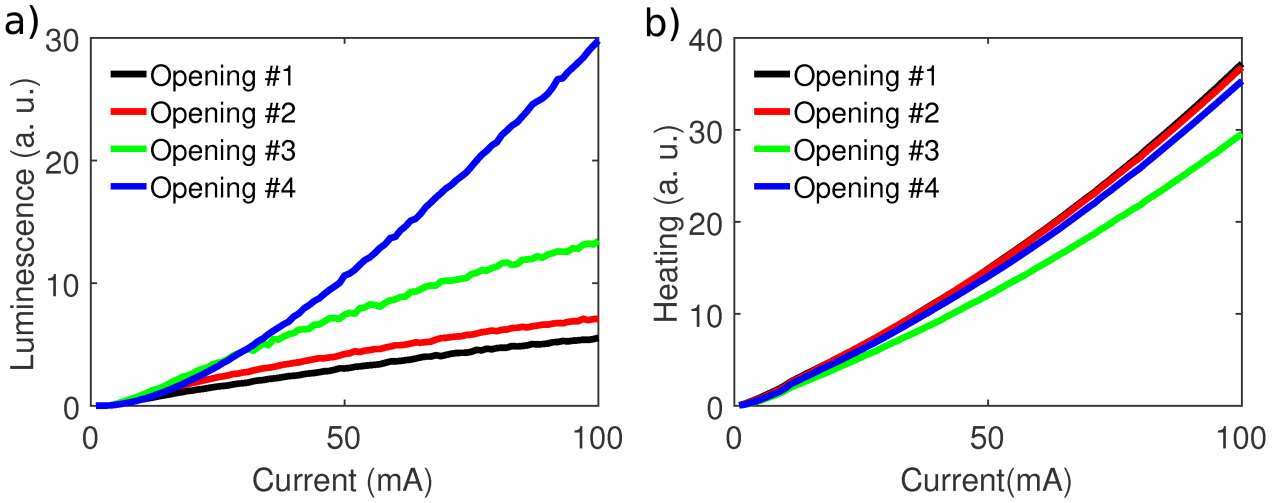

Figure 3. (a) Luminescence and (b) temperature as a function of the injected current in selected areas of the DDS device. First opening corresponds to the center of the structure, and the last to the outer ring outside the metal contact. (color online)

Fig. 4 shows the optical and thermal signals for different currents as a function position, as obtained by interpolating the signals for the metal covered regions. Fig. 4-a) shows that at low currents the luminescence has a maximum at the center and the luminescence is reduced towards the edge. At larger current densities the situation becomes reversed and the maximum shifts to the outer ring of the mesa, again suggesting that current spreading and crowding play an important role in the operation of the structure. For the heat distribution profile in Fig. 4b, the temperature differences are again relatively small but at large currents an increased contribution at the mesa edge appears, potentially suggesting that surface recombination may affect the device operation. Evidently, however, the origin and effects of the heating still need further investigations, as they are affected by

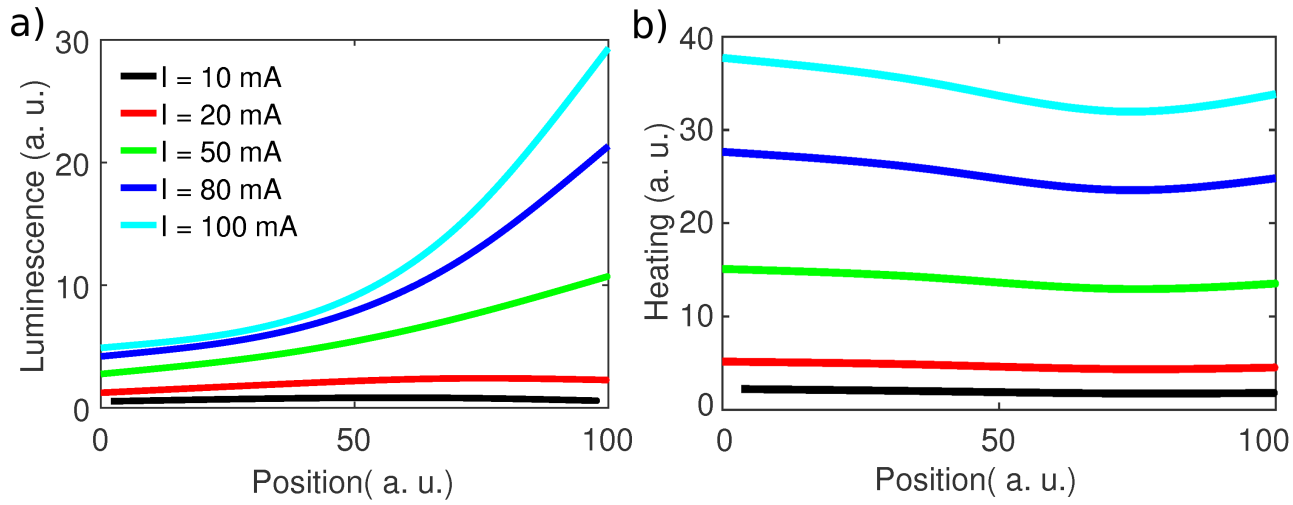

Figure 4. (a) Luminescence and (b) temperature as a function of position along the DDS structure for selected injection currents. Zero position corresponds to the center of the structure. (color online)

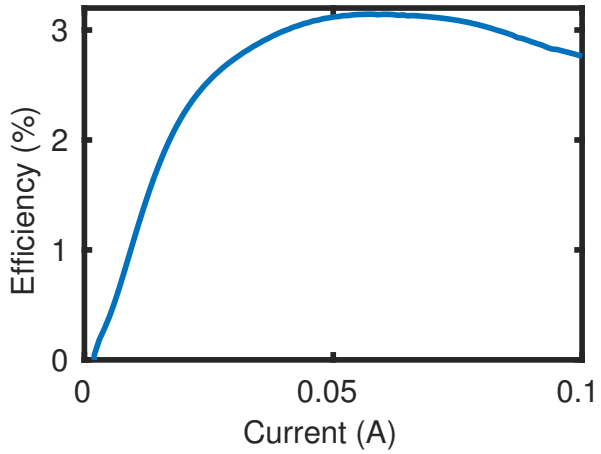

Figure 5. The average efficiency of the DDS sample as a function of injection current as estimated using the thermal and luminescence data, averaged over the whole device area. (color online)

several effects that are not fully accounted for by our present analysis or the model of Section 2. These include e.g. ohmic losses in the current spreading layers, possible emissivity modulation of semiconductor layers that are partly transparent to near infrared radiation and, in particular, possible thermal transport effects within the mesa that could be expected to lead to larger heating of the mesa center if the heat is not efficiently dissipated into the substrate.

Finally, Fig. 5 shows the estimated external quantum efficiency of the whole structure as calculated using whole mesa area as the single computation domain in Eq. (8). At very small currents the efficiency approaches zero, presumably due to the combined effect of nonradiative recombination dominating over the radiative recombination and possible nonidealities (such as the weak hotspot seen in Fig. 2) of the diode. The efficiency peaks at about 3% at approximately 50 mA and starts to decrease at larger current densities. While the external quantum efficiency of 3% would be low for an actual light emitting diode whose internal quantum efficiency is expected to be quite high, it should also be noted that light extraction from the present device is extremely inefficient: the metal contacts cover approximately 70% of the device top surface and the most significant part of light emission most likely takes place through the mesa edges. As the typical light extraction efficiency of

a planar semiconductor surface due to total internal reflections is of the order of 2%, the estimated external quantum efficiency sounds even slightly higher than expected, even when considering the edge emission and photon recycling effects affecting the efficiency.

5. CONCLUSIONS

We explore combining thermal imaging with optical imaging to provide an alternative noncontact calorimetric efficiency measurement technique that can also provide spatially resolved information on the device performance. The approach has allowed us to extend the calorimetric efficiency measurement techniques to use thermal imaging and to directly observe the non-uniform distribution of light-emission across the studied DDS devices, primarily resulting from current crowding, as well as to observe possible signatures of surface recombination at structure edges. While the proposed model for measuring the spatially resolved quantum efficiency still requires further development, we have shown that the combination of LIT and visible imaging can be used for making calibrated calorimetric efficiency measurements and may provide useful additional insight to the spatial efficiency and light emission distributions of light emitting devices.

ACKNOWLEDGMENTS

This project has received funding from the Academy of Finland and the European Research Council (ERC) under the European Unions Horizon 2020 research and innovation programme (grant agreement No 638173). We acknowledge the provision of facilities and technical support by Aalto University at Micronova Nanofabrication Centre.

REFERENCES

[1] Sheik-Bahae, M. and Epstein, R. I., "Optical refrigeration," *Nature Photonics* **1**, 693 – 699 (Dec. 2007).

[2] Oksanen, J. and Tulkki, J., "Thermophotonic heat pumpa theoretical model and numerical simulations," *Journal of Applied Physics* **107**(9), 093106 (7 p.) (2010).

[3] Dunstan, D. J., "On the measurement of absolute radiative and non-radiative recombination efficiencies in semiconductor lasers," *Journal of Physics D: Applied Physics* **25**, 1825 – 1828 (Dec. 1992).

[4] Bender, D. A., Cederberg, J. G., Wang, C., and Sheik-Bahae, M., "Development of high quantum efficiency GaAs/GaInP double heterostructures for laser cooling," *Applied Physics Letters* **102**(25), 252102 (4 p.) (2013).

[5] Olsson, A., Tiira, J., Partanen, M., Hakkarainen, T., Koivusalo, E., Tukiainen, A., Guina, M., and Oksanen, J., "Optical Energy Transfer and Loss Mechanisms in Coupled Intracavity Light Emitters," *IEEE Transactions on Electron Devices* **63**, 3567–3573 (Sept. 2016).

[6] Breitenstein, O., Warta, W., and Langenkamp, M., [*Lock-in Thermography*], vol. 10 of *Springer Series in Advanced Microelectronics*, Springer Berlin Heidelberg, Berlin, Heidelberg (2010).

[7] Gfroerer, T. H., Cornell, E. A., and Wanlass, M. W., "Efficient directional spontaneous emission from an InGaAs/InP heterostructure with an integral parabolic reflector," *Journal of Applied Physics* **84**(9), 5360 (1998).

[8] Vargas, H. and Miranda, L., "Photoacoustic and related photothermal techniques," *Physics Reports* **161**, 43–101 (Apr. 1988).

[9] Wang, C., Li, C.-Y., Hasselbeck, M. P., Imangholi, B., and Sheik-Bahae, M., "Precision, all-optical measurement of external quantum efficiency in semiconductors," *Journal of Applied Physics* **109**(9), 093108 (10 p.) (2011).